A&A 610, A34 (2018)
DOI: 10.1051/0004-6361/201731864
© ESO 2018

Astronomy & Astrophysics

Glimpses of the past activity of Sgr A⋆ inferred from X-ray echoes in Sgr C

D. Chuard[1,2], R. Terrier[2], A. Goldwurm[1,2], M. Clavel[3], S. Soldi[2], M. R. Morris[4], G. Ponti[5], M. Walls[6], and M. Chernyakova[6,7]

[1] Irfu/Département d'astrophysique, CEA Paris-Saclay, Orme des Merisiers, 91191 Gif-sur-Yvette, France
e-mail: dimitri.chuard@cea.fr
[2] APC, Univ. Paris Diderot, CNRS/IN2P3, CEA/Irfu, Obs. de Paris, USPC, 75205 Paris Cedex 13, France
[3] Space Sciences Laboratory, 7 Gauss Way, University of California, Berkeley, CA 94720-7420, USA
[4] Dep. of Physics and Astronomy, University of California, Los Angeles, CA 90095, USA
[5] Max-Planck-Institut für extraterrestrische Physik, 85748 Garching, Germany
[6] School of Physical Sciences, Dublin City University, Glasnevin, Dublin 9, Ireland
[7] Dublin Institute of Advanced Studies, 31 Fitzwilliam Place, Dublin 2, Ireland

Received 30 August 2017 / Accepted 21 November 2017

ABSTRACT

Context. For a decade now, evidence has accumulated that giant molecular clouds located within the central molecular zone of our Galaxy reflect X-rays coming from past outbursts of the Galactic supermassive black hole. However, the number of illuminating events as well as their ages and durations are still unresolved questions.
Aims. We aim to reconstruct parts of the history of the supermassive black hole Sgr A⋆ by studying this reflection phenomenon in the molecular complex Sgr C and by determining the line-of-sight positions of its main bright substructures.
Methods. Using observations made with the X-ray observatories *XMM-Newton* and *Chandra* between 2000 and 2014, we investigated the variability of the reflected emission, which consists of a Fe Kα line at 6.4 keV and a Compton continuum. We carried out an imaging and a spectral analysis. We also used a Monte Carlo model of the reflected spectra to constrain the line-of-sight positions of the brightest clumps, and hence to assign an approximate date to the associated illuminating events.
Results. We show that the Fe Kα emission from Sgr C exhibits significant variability in both space and time, which confirms its reflection origin. The most likely illuminating source is Sgr A⋆. On the one hand, we report two distinct variability timescales, as one clump undergoes a sudden rise and fall in about 2005, while two others vary smoothly throughout the whole 2000−2014 period. On the other hand, by fitting the Monte Carlo model to the data, we are able to place tight constraints on the 3D positions of the clumps. These two independent approaches provide a consistent picture of the past activity of Sgr A⋆, since the two slowly varying clumps are located on the same wavefront, while the third (rapidly varying) clump corresponds to a different wavefront, that is, to a different illuminating event.
Conclusions. This work shows that Sgr A⋆ experienced at least two powerful outbursts in the past 300 yrs, and for the first time, we provide an estimation of their age. Extending this approach to other molecular complexes, such as Sgr A, will allow this two-event scenario to be tested further.

Key words. Galaxy: center – ISM: clouds – X-rays: ISM

1. Introduction

From our terrestrial outlook, the astrophysical phenomena occurring at the centre of the Milky Way are observable at an unrivalled level of detail because the nucleus of our Galaxy is the closest we can study by two orders of magnitude. Consequently, the centre of the Milky Way has emerged as a key prototype for the study of galactic nuclei. In particular, like most massive galaxies, the Milky Way hosts a supermassive black hole at its centre, named after its electromagnetic counterpart, the compact radio source Sagittarius A⋆ (Sgr A⋆) discovered by Balick & Brown (1974). It is located around 8 kpc from Earth, and its mass is about four million times that of the Sun (see Chatzopoulos et al. 2015; Boehle et al. 2016, for recent estimates). Nevertheless, in contrast with active galactic nuclei (AGN), its emission is extremely faint. In X-rays (2–10 keV), its absorption-corrected quiescent luminosity is about 10^{33} erg s^{-1} (Baganoff et al. 2003), which is not only several orders of magnitude below the Eddington limit, but also far lower than what is expected from black-hole feeding by the stellar winds in its vicinity (Genzel et al. 2010). A strong effort is being made to account for this underluminous state using numerical models of the gas dynamics (e.g. Cuadra et al. 2015; Mościbrodzka 2017). In particular, radiatively inefficient accretion flow (RIAF) models are in very good agreement with the observations of the steady-state emission from Sgr A⋆ (Wang et al. 2013).

The black hole also undergoes regular flare-like events, especially in X-rays (Neilsen et al. 2013; Ponti et al. 2015; Yuan & Wang 2016; Ponti et al. 2017, and references therein). During these episodes, its luminosity can increase by up to two orders of magnitude above the quiescent value. This variability indicates that significant changes in the accretion flow, such as stochastic acceleration, shocks, magnetic reconnection, or tidal disruption of small bodies, are possible. By extrapolation, we

may therefore infer that Sgr A* sporadically ventures out of its current low-luminosity state. The idea that this could have occurred in the past motivates the search for relics of potential past high-activity episodes in the interstellar medium surrounding the central black hole (see Ponti et al. 2013, for a review).

When an X-ray source experiences an intense burst, it is indeed possible to track it long after it ends by monitoring its reflection on any optically thick molecular material located along the trajectory of the photons. This reflected emission consists of a strong fluorescent line of neutral and low-ionised iron (Fe Kα) at 6.4 keV, together with much weaker lines of lower atomic number elements and a continuum component produced by Compton scattering. In the case of potential past flares of Sgr A*, this emission is expected to come primarily from the giant molecular clouds populating the central molecular zone (CMZ; Morris & Serabyn 1996; Sunyaev et al. 1993).

In 1994, the ASCA mission first detected a strong Fe Kα signal in Sgr B2, the most massive molecular cloud in the Galaxy, which is located at a projected distance of about 100 pc from Sgr A* (Koyama et al. 1996). Since then, similar detections have been reported at many other locations in the CMZ (e.g. Nobukawa et al. 2008; Terrier et al. 2018). Notwithstanding that this non-thermal emission can also be produced by low-energy cosmic rays (LECR; e.g. Yusef-Zadeh et al. 2002; Dogiel et al. 2009; Tatischeff et al. 2012), the great variability observed in the Sgr A complex (Muno et al. 2007; Ponti et al. 2010; Capelli et al. 2011; Clavel et al. 2013, 2014) and in Sgr B2 (Koyama et al. 2008; Inui et al. 2009; Terrier et al. 2010; Nobukawa et al. 2011) is a solid argument for a reflection origin.

Considering the estimated energetics of the illumination, the most plausible explanation is that the source is Sgr A*. Therefore, it is possible to probe the past activity of the Galactic supermassive black hole over the past few centuries by monitoring the echoes of its past flares while they propagate through the CMZ. The current distribution and evolution of the 6.4 keV bright clumps indeed suggest that Sgr A* experienced at least one, and probably two, powerful outbursts ($L \sim 10^{39}$ erg s^{-1}) in the past few centuries (Clavel et al. 2013). However, this does not allow a proper reconstruction of the past light curve of Sgr A* as long as the distances between the bright clumps and the black hole, and hence the propagation delay, remain unknown. Two main approaches have emerged to address this problem: correlating variations between multiple regions all over the CMZ while assuming that they are illuminated by the same event on the one hand (Clavel et al. 2013; Churazov et al. 2017; Terrier et al. 2018), and using the physical properties of the X-ray emission to constrain the line-of-sight positions of individual clumps on the other hand (Capelli et al. 2012; Ryu et al. 2013; Walls et al. 2016).

From this standpoint, the molecular complex Sgr C is a highly valuable object of study as it allows the two methods to be applied together for the first time. Sgr C is indeed a suitable candidate for three-dimensional position determination based on spectral analysis as its clumps are well resolved. It is also ideally located for studying correlations in the Fe Kα emission from both sides of the Galactic plane, since Sgr C and Sgr B2 are on opposite sides of Sgr A* at similar projected distances.

Fe Kα line emission at 6.4 keV was first detected in Sgr C by Murakami et al. (2001) with ASCA. It was then resolved into four main clumps by Nakajima et al. (2009) with *Suzaku*. Furthermore, the study of the thermal diffuse X-ray emission by Tsuru et al. (2009) revealed an elliptical object designated as G359.41−0.12 and an adjacent chimney-like structure. These two features, which are notably bright in the SXV Kα line at 2.45 keV, are thought to be a supernova remnant (SNR) candidate and its associated outflow. Many non-thermal radio filaments are also found in the area, including one of the brightest in the CMZ, the Sgr C filament (Liszt 1985; Anantharamaiah et al. 1991; LaRosa et al. 2000), as well as two non-thermal X-ray filaments that may be two pulsar wind nebulae (Chuard et al. 2017). Because of the possible interaction of all these structures with the 6×10^5 $M_\odot$ of molecular gas contained in Sgr C (Liszt & Spiker 1995), some of its Fe Kα emission may be due to cosmic-ray irradiation rather than X-ray reflection. Therefore Sgr C offers a unique opportunity to study these two competing scenarios for the origin of the Fe Kα emission.

We study the variability of the Fe Kα emission in observations of Sgr C made with the X-ray observatories *XMM-Newton* and *Chandra* between 2000 and 2014 (Sect. 2). To do so, we used both imaging analysis and light curve extraction (Sect. 3). Based on our results, we discuss the plausibility of the reflection scenario compared to the cosmic-ray irradiation scenario. Finally, by comparing our data to Monte Carlo simulated reflection spectra, we are able to place the best constraints to date on the line-of-sight positions of the main bright clumps of Sgr C (Sect. 4.1). Ultimately, extending this approach with the inclusion of other molecular complexes allows us to partially reconstruct the past light curve of the Galactic supermassive black hole (Sect. 4.2).

2. Observations and data reduction

Sgr C has been repeatedly observed with *XMM-Newton* and *Chandra*, during either dedicated pointings or CMZ scans. We consider here all the available observations from these two satellites, including the latest *Chandra* observation that we were granted in 2014. All data were taken with focal plane imaging spectrometers using X-ray CCDs, namely the European Photon Imaging Camera (EPIC) onboard *XMM-Newton* (Turner et al. 2001; Strüder et al. 2001) and the *Chandra* Advanced CCD Imaging Spectrometer (ACIS; Garmire et al. 2003). They represent a final dataset of 14 observations, covering the period from September 2000 to August 2014 (Table 1).

The data reduction was carried out using the standard tools provided for each observatory, the *XMM-Newton* Extended Source Analysis Software (ESAS; Snowden et al. 2008) included in the *XMM-Newton* Science Analysis Software (SAS) version 12.0.1, and the *Chandra* Interactive Analysis of Observations software (CIAO; Fruscione et al. 2006) version 4.8, respectively.

Exposure-corrected images were created from *Chandra* data using the CIAO scripts `fluximage` and `merge_obs`. Only ACIS-I chips were considered. We excluded events within a circular region of radius 2.76′ centred on $(l, b) = (359.56°, -0.08°)$ in the 2005 dataset because of contamination from the X-ray binary KS 1741−293, which was very active at that time (Degenaar & Wijnands 2013). Maps of the Fe Kα emission were generated by integrating the counts in the band 6.32−6.48 keV and continuum-subtracted following the approach of Ponti et al. (2010) and Clavel et al. (2013). The underlying continuum emission was estimated from images created in the 4.0−6.1 keV band, assuming a power-law spectrum of photon index $\Gamma = 2$ (i.e. with a rescaling factor of 0.045).

Source spectra were extracted from *Chandra* data using the CIAO `specextract` routine, which also generated the ancillary response file (ARF) and the redistribution matrix file (RMF). It was also used to extract background spectra from blank sky event files, which were created by combining observations of relatively

Table 1. List of all *XMM-Newton* (EPIC) and *Chandra* (ACIS-I) observations, grouped into the six periods we defined to study the time variability (Fig. 2).

Date	Obs. ID	Exposure Time (ks)		
		EPIC-MOS	EPIC-pn	ACIS-I
2000-09-11	0112970701	23.89	20.00	–
2000-09-21	0112970801	23.89	20.00	–
2005-07-22	5892	–	–	97.91
2006-02-27	0302883101	11.47	9.84	–
2006-09-09	0302884501	8.42	6.79	–
2007-09-06	0504940701	6.67	5.06	–
2008-03-04	0511001301	6.67	5.06	–
2008-09-27	0511001401	6.67	5.03	–
2012-08-30	0694640201	46.67	45.04	–
2012-09-07	0694640101	43.67	42.04	–
2012-09-12	0694640901	44.67	43.04	–
2014-07-29	16174	–	–	30.10
2014-08-01	16642	–	–	29.81
2014-08-03	16643	–	–	35.62

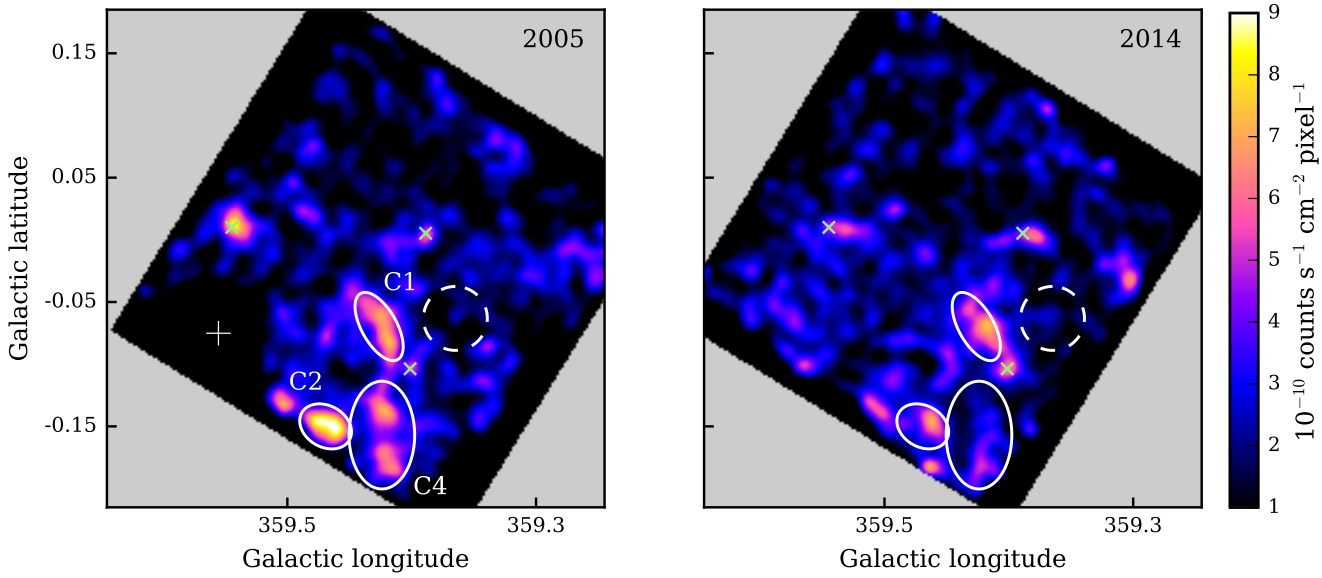

Fig. 1. *Chandra* continuum-subtracted images of the Fe Kα emission in Sgr C for the observations taken in 2005 (*left*) and 2014 (*right*). The maps are in units of counts s^{-1} cm^{-2} pixel^{-1} with a pixel size of about 1″, and smoothed using a Gaussian kernel of 20-pixel radius. The regions of interest (Sgr C1, Sgr C2, and Sgr C4) are marked by the solid ellipses (see Table 2). The dashed circle shows the control region. The white cross marks the position of the X-ray transient KS 1741−293, which has been removed from the 2005 dataset. The green crosses mark the positions of bright point sources ($F_{0.5-8\,\mathrm{keV}} > 10^{-5}$ counts s^{-1} cm^{-2}) from the catalogue of Muno et al. (2006) that remain visible in the 6.4 keV band after continuum subtraction.

empty fields available from the *Chandra* calibration database (CALDB version 4.7.2). *XMM-Newton* spectra were extracted with the ESAS `mos-spectra` and `pn-spectra` scripts. Filter-wheel closed event lists from the ESAS calibration database were used to estimate the quiescent particle background. All spectra were then analysed with *Sherpa*, the modelling and fitting package of CIAO (Freeman et al. 2001). They were re-binned until the square root of the number of counts in each bin exceeded a minimum signal-to-noise ratio, between 3 and 10, depending on the quality of the spectrum. The analysis was restricted to the energy range 2–7.5 keV. Model fits were carried out using a chi-square statistic with the Gehrels variance function (Gehrels 1986). In the following, all errors are given at 1σ (68% confidence) level and descriptions implicitly refer to Galactic coordinates.

3. Variability of the Fe Kα emission

We first focus on the spatial distribution of the Fe Kα emission in Sgr C. In order to identify the brightest regions and track them over time, we took advantage of *Chandra*'s unique imaging capabilities thanks to its high angular resolution. We produced two images of the Fe Kα emission from our dataset from the data taken in 2005 and 2014, respectively (Fig. 1). Both correspond to an exposure time of about 100 ks (see Table 1).

Three main bright regions are visible in the 2005 image. They match those identified by Nakajima et al. (2009) using *Suzaku* data taken in Feburary 2006 (seven months later than the first ACIS-I *Chandra* data). These regions (indicated as Sgr C1, Sgr C2, and Sgr C4; see also Table 2) are known to be coincident with molecular structures seen in radio

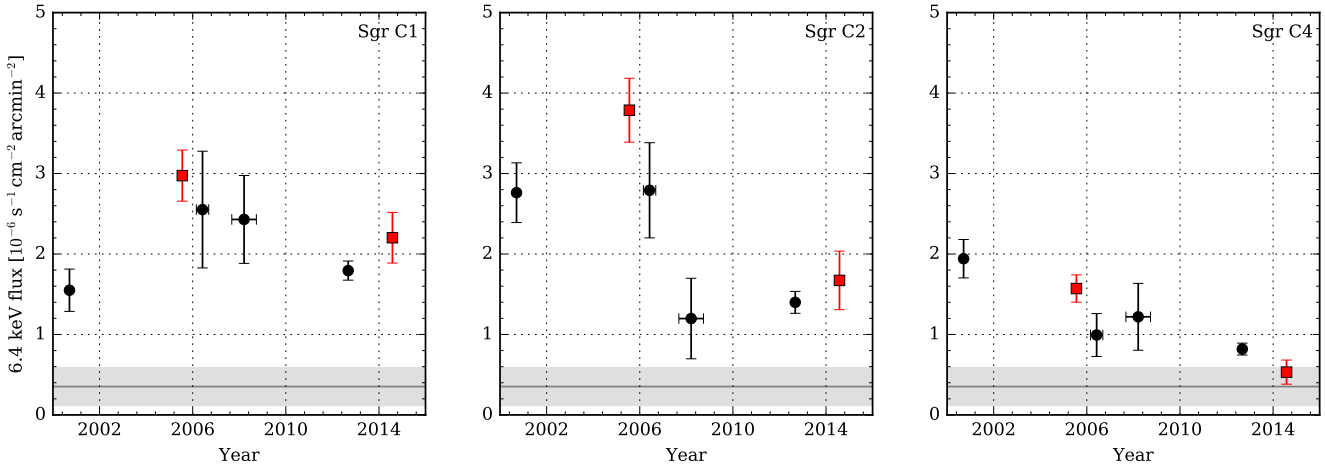

Fig. 2. Light curves of the 6.4 keV line emission obtained by fitting the phenomenological model and integrated over the regions Sgr C1 (*left*), Sgr C2 (*centre*) and Sgr C4 (*right*). The black circles and the red squares correspond to *XMM-Newton* and *Chandra* observations, respectively. The grey shaded bars show the average level of background emission measured in the control region (their thickness represents one standard deviation).

Table 2. Galactic coordinates of the elliptical regions, following the naming convention of Ryu et al. (2013) and Terrier et al. (2018).

Name	l (°)	b (°)	Axes (′)	Angle (°)
Sgr C1	359.43	−0.07	3.66, 1.69	119
Sgr C2	359.47	−0.15	2.64, 1.99	150
Sgr C4	359.42	−0.16	5.20, 3.17	90
Control	359.36	−0.06	3.08, 3.08	–

Notes. Sgr C3 is out of the *Chandra* field of view and therefore not considered here.

(Ryu et al. 2013; Terrier et al. 2018). Between 2005 and 2014, the morphology of the Fe Kα emission underwent noticeable changes. The image built from the 2014 data reveals that there is almost no more emission in Sgr C4. Sgr C2, the brightest region in 2005, is also clearly less luminous, and the centroid of the bright area is shifted towards the west. The case of C1 is more complicated as the peak value of the radiance remains roughly constant, but the bright area shrinks and moves towards the west as well. Thus, all three regions exhibit clear variability. These results based on *Chandra* data are therefore in full agreement with the findings of Terrier et al. (2018) using *XMM-Newton* observations.

In order to obtain more quantitative information about the variability, we carried out a spectral analysis in the three main regions identified above (Table 2). Following the standard approach, we fitted the spectra extracted in these regions with a phenomenological model composed of a reflected emission component and two thermal plasma components (APEC; Smith et al. 2001). The reflected emission was modelled by an absorbed (with fixed column density of $N_{\rm H} = 10^{23}$ cm^{-2}) power law of photon index $\Gamma = 2$ and a Gaussian line with $E = 6.4$ keV and $\sigma_E = 10$ eV. The power law corresponds to the spectrum of the illuminating source, and the absorption is the result of the crossing of the molecular cloud. Following Koyama et al. (2007) and Tsuru et al. (2009), the temperatures of the two APEC models were fixed at 1.0 and 6.5 keV, respectively, the first accounting for the soft local plasma emission and the second for the hot Galactic ridge emission (Worrall et al. 1982). No fixed normalisation ratio was assumed between the two APEC components, which were thus left free to vary. We fixed the metallicity to solar values (following Nakajima et al. 2009) and applied foreground interstellar absorption (with column density fixed at $N_{\rm H} = 7.5\times10^{22}$ cm^{-2}) to all components except for the Gaussian line:

$$\texttt{wabs}_1 \times (\texttt{apec}_1 + \texttt{apec}_2 + \texttt{wabs}_2 \times \texttt{powerlaw}) + \texttt{gaussian}. \quad (1)$$

Even if this description is not fully physically relevant (see Sect. 4.1), it allows us to precisely measure the flux in the Fe Kα line.

The dataset including all available *XMM-Newton* and *Chandra* observations was split into six periods (see Table 1) in order to study the flux variability over time. For each region, the observations for all these six periods were fitted simultaneously, leaving the normalisation of the reflection components free to vary from one period to another, while the thermal components were held constant over time. The same approach was then applied to a control region (Table 2) that did not overlap the bright clumps in order to estimate the level of background emission at 6.4 keV. The reduced chi-square is very close to 1 for all fits.

The Fe Kα light curves we derived are shown in Fig. 2. There is no evidence of a systematic shift between *XMM-Newton* and *Chandra* data points, suggesting that intercalibration errors, although possible, do not significantly affect our results. The observed trend confirms that the reflected emission from Sgr C has varied significantly for the past 15 yrs. In Sgr C2 and C4, the hypothesis that the flux has been constant during the entire period is rejected at 5.6 and 5.4σ, respectively. The light curve of Sgr C2 exhibits a maximum in 2005, followed by a sharp decrease and a residual flux consistent with constant emission from 2008 to 2014. However, since no data were collected between 2000 and 2005, it is possible that the flux of Sgr C2 was even higher during this period. The light curve of Sgr C4 is compatible with a linear decrease over the whole period down to the background level indicated by the grey band. As for Sgr C1, its light curve would have been compatible with a constant without the excess seen by *Chandra* in 2005 (+62% compared to the 2005-excluded average). In this respect, it is worth noting that the variability we infer from the light curves only takes changes in intensity into account and thus might be hiding changes in morphology within the region of integration (Clavel et al. 2013). This appears to be especially true for Sgr C1, whose 6.4 keV emission morphology evolves, but with almost constant brightness.

The timescale and the amplitude of the variability detected at 6.4 keV exclude the cosmic-ray irradiation scenario and

confirm the reflection origin of the Fe Kα emission in Sgr C, in agreement with Terrier et al. (2018). The fluxes in the line and in the reflected continuum appear to be positively correlated at the 4σ level (determined by permutation following Legendre & Legendre 1998, to take uncertainties in both variables into account), which is also consistent with the reflection scenario. Furthermore, the apparent motion of the emission centroids towards the west, that is, away from Sgr A⋆, may be evidence of the signal propagation within these clouds. In the following, we therefore consider that Sgr A⋆ is the source at the origin of this reflected emission (see also Sect. 5).

4. Constraints on the past activity of Sgr A⋆

4.1. Determining the line-of-sight positions of the clumps

It is possible to use the observations of Sgr C to place constraints on the past light curve of Sgr A⋆ on the condition that we can precisely determine the positions of the bright clumps along the line of sight. This information can be extracted from the cloud X-ray spectra but, until recently, no relevant physical models were available for this purpose. Either phenomenological models (like the one we used in Sect. 3) or models developed for other geometries, e.g. `MyTorus` (Zhang et al. 2015; Mori et al. 2015) and `pexrav` (Ponti et al. 2010), were used. These poorly suited models stongly limit any inference of the physical parameters of the reflection phenomenon and may provide results that are marred by significant systematic errors. Fortunately, Monte Carlo models computing the spectrum produced by X-ray reflection from a spherical molecular cloud have been recently developed. They are thus the best-suited models available to date to physically describe the reflection phenomenon.

We used a Monte Carlo spectral model developed by Walls et al. (2016), hereafter referred to as the Monte Carlo model, to determine the line-of-sight positions of the reflecting clouds from their spectra. This model has been designed to take the geometry of the reflection, which has a major influence on the flux and spectral shape of the cloud emission (Walls et al. 2016), into account. The geometry is parametrised in the model by the angle between the cloud, the illuminating source, and the observer, referred to as the line-of-sight angle. The total continuum flux at low energies notably increases with this angle because photons only superficially penetrate the cloud before being scattered towards the observer. Consequently, the scattered photons are more likely to be absorbed in the low-angle case than in the high-angle case. The line-of-sight angle, as well as the cloud column density, also affect the strength of the Fe Kα line and the depth of the iron edge (Walls et al. 2016). All these effects are of key interest for the line-of-sight position determination.

The line-of-sight angle and the cloud column density are free parameters of the Monte Carlo model that can thus be constrained through a spectral fitting procedure based on our dataset. In order to have the best possible constraints on their values, we restricted our analysis to the deepest observations (2000, 2005, 2012, and 2014). We used the same model as in Sect. 3, except that the reflected emission was now modelled using the Monte Carlo model:

$$\texttt{wabs} \times (\texttt{apec}_1 + \texttt{apec}_2 + \texttt{montecarlo}). \quad (2)$$

The parameters of the two thermal plasma components and of the foreground interstellar absorption were kept unchanged (see Sect. 3). For a given region and a given period, the normalisation was left free to vary. The line-of-sight angle and the cloud column density (with a uniform density profile) were also left free but constant over all periods. The dataset allows good parameter constraints with satisfactory fit quality (see Fig. 3 and Table 3). The variability of the reflected component is found to be consistent with the light curves obtained in Sect. 3.

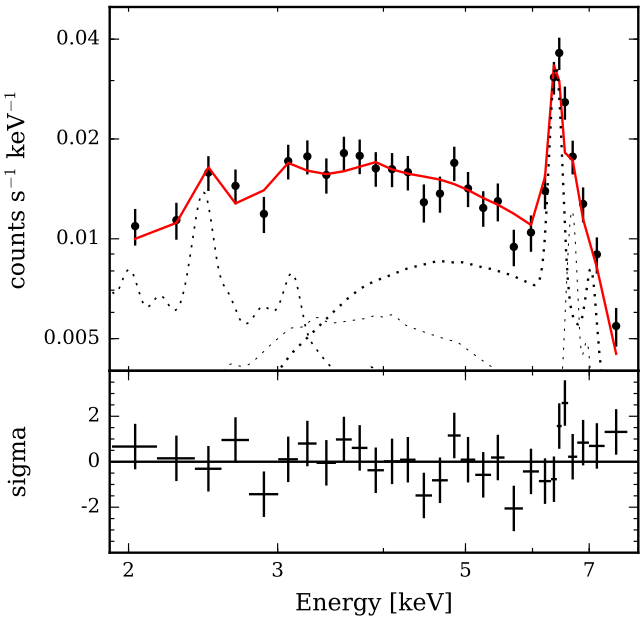

Fig. 3. Spectrum of Sgr C1 observed with EPIC-pn onboard *XMM-Newton* in 2012. The red line corresponds to the best-fit model. The dotted lines show the three components of the model: the hot (thin line) and soft (medium) thermal plasmas, and the Monte Carlo reflected emission (thick).

Table 3. Values of the line-of-sight angles and uniform cloud column densities, obtained by fitting the *XMM-Newton* and *Chandra* data with the Monte Carlo model.

Region	Angle (°)	$N_{\rm H}$ (10^{23} cm^{-2})	χ^2/d.o.f.
Sgr C1	$102.0^{+5.8}_{-11.5}$	$2.18^{+0.20}_{-0.37}$	423.6/372
Sgr C2	$66.7^{+9.9}_{-6.3}$	$7.0^{+1.2}_{-1.2}$	234.0/206
Sgr C4	$96.0^{+6.2}_{-9.5}$	$1.63^{+0.12}_{-0.13}$	436.2/420

Notes. The metallicity is set to solar values.

The best-fit values of the cloud parameters are given in Table 3. The column densities we find are higher than previous estimates (Yusef-Zadeh et al. 2007; Nakajima et al. 2009). As Walls et al. (2016) reported similar findings for Sgr B2, this suggests that prior modelling efforts might have been biased towards underestimating column densities. In the case of Sgr C2, the difference is almost one order of magnitude. However, our values are in the range of those inferred from the CS J = 1–0 line emission ($N_{\rm H} \sim 10^{23}$ cm^{-2}; Tsuboi et al. 1999) and from *Herschel* far-infrared data ($N_{\rm H} \sim 10^{24}$ cm^{-2}; Molinari et al. 2011).

Using the angles obtained from the fits and the celestial coordinates, we are able to derive the 3D positions of the clumps within the CMZ (Fig. 4). Sgr C2 is found to be in front of Sgr A⋆, while C1 and C4 are slightly behind it, both at comparable line-of-sight distances. Although the error bars look rather small, one should keep in mind that some systematics may affect our results, notably because of the uncertainty on the cloud metallicity, its density profile, and its geometry.

We tested the effect of the cloud metallicity Z. Three values that are higher than solar are parametrised in the model (1.3,

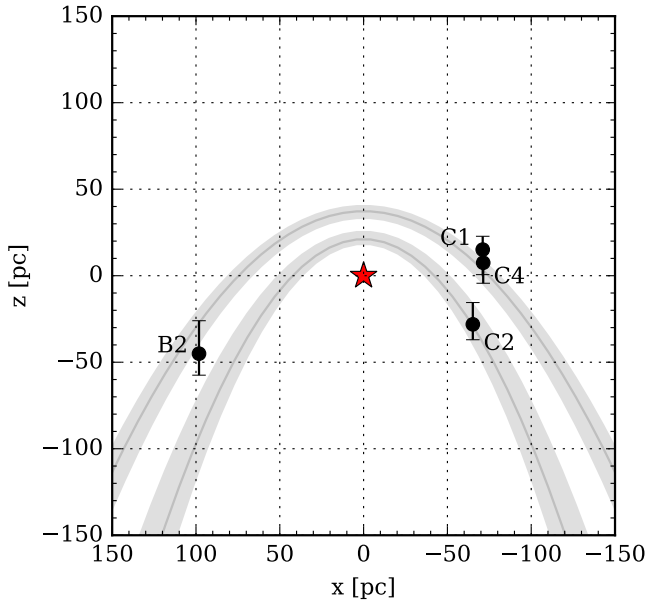

Fig. 4. Face-on view of the Galactic centre. The negative direction along the z-axis points towards Earth. The red star marks the position of Sgr A*. The black dots show the best-fit positions for the bright clumps Sgr C1, C2, C4 (Table 3), and Sgr B2 (Walls et al. 2016) in the solar-metallicity and uniform density profile case. The grey parabolas trace the best-fit associated wavefronts (as seen from Earth; Sunyaev & Chuarzov 1998) for the two-event model. The width of the parabolas represents the statistical uncertainty on the position, not the duration of the associated event.

1.7, and 1.9) but we only considered the $Z = 1.3$ case since the Galactic centre abudances are known to be close to solar (see e.g. Davies et al. 2009). We find than increasing the metallicity tends to separate the clouds more from each other. In the case of Sgr C1, we observe that the line-of-sight angle increases with increasing Z up to $107.0^{+9.2}_{-13.1}$ degrees. Conversely, the angle of Sgr C2 decreases to $60.0^{+4.9}_{-8.2}$ degrees. The position of Sgr C4 remains almost unchanged ($93.0^{+15.6}_{-15.1}$ degrees). Although some of these fits are statistically less good than those with $Z = 1$, this procedure allows us to estimate the typical systematic error that results from the uncertainty on metallicity. On the whole, we find that when we assume a higher metallicity, this does not fundamentally alter the trend of our results even if it marginally changes the angle values.

In addition, the shape of the cloud and its density profile might not be as assumed by the Monte Carlo model. We tested Gaussian density profiles. They have a very limited effect on our findings. The line-of-sight angle changes by only a few degrees for Sgr C1 and C2 and remains unchanged for Sgr C4. Moreover, all the fits with Gaussian profiles are statistically less good than those with uniform density. Consequently, we did not consider these alternative profiles further.

The cloud might also be only partially illuminated if the burst duration is shorter than the cloud light-crossing time, which might be the case for Sgr C2 according to the rapid change observed in its light curve (Fig. 2). Ultimately, the line-of-sight geometry of the cloud would also be required in order to translate the observed light curves into the original burst profile. Unfortunately, no satisfying heuristic can be found to estimate the influence of these parameters. It would require a refined version of the Monte Carlo model, which is not yet available.

Despite these limitations, the position and column density we find for Sgr C2 agree well with those required to account for the extinction of the north-eastern portion of the SNR candidate G359.41−0.12 (Chuard et al. 2017). It is also worth noting that while some of the 6.4 keV emission in Sgr C4 is superposed upon the SNR candidate emission, there is no sign of absorption of the SNR candidate emission by Sgr C4. As a consequence, G359.41−0.12 may consistently be located somewhere between Sgr C2 and Sgr C4. Finally, our results also agree with the work of Sawada et al. (2004), recently confirmed by Yan et al. (2017), who derived a distribution of the molecular clouds in the Galactic centre that is compatible with the positions we find for the main subregions of Sgr C.

Nevertheless, our results are significantly different from previous estimates that were based on partial absorption of the local plasma emission reported by Ryu et al. (2013). The origin of this discrepancy is unclear. The model used by previous studies to describe the reflected spectrum coming from the illuminated cloud (an absorbed power law) is poorly suited, as was shown by Walls et al. (2016). In particular, the strong dependence of the spectrum on the line-of-sight angle can hamper the partial absorption measurement if it is not properly modelled. Furthermore, we note that since the molecular cloud only covers part of the region chosen for the spectral analysis, a fraction of the flux is not in the line of sight of the cloud. Hence, part of the absorption is independent of the cloud location, and it is inaccurate to consider the cloud density liable for all the absorption of the thermal plasma in the region. This is another important bias in the derivation of the cloud position from the fitted absorption fraction as done by Ryu et al. (2013).

4.2. Investigation of the associated illuminating events

Constraining the 3D positions of the clouds within the CMZ opens the door to reconstructing the past light curve of Sgr A*. To do so, we developed a proxy of the Monte Carlo model to fit the time delay of the associated echo directly instead of the line-of-sight angle. Considering that Sgr C1, C4 and B2 are roughly located on the same parabola, we tested two hypotheses: (i) that all clumps result from the same event; and (ii) that the illumination in Sgr C2 is due to a second event. Following the Occam razor parsimony principle, we restricted our analysis to one-event and two-event models. We did not consider models with more events to avoid overfitting.

We first fitted the spectra with the proxy model while imposing the same value of the delay on all clumps. Cloud column densities were fixed to the best-fit values we found when fitting each clump individually to ensure stability in the parameter estimation. Then, we repeated the procedure, now assuming that Sgr C2 corresponds to a different delay. We compared the statistics of these two fits using a likelihood-ratio test and found that the second hypothesis is statistically better than the first ($p < 0.05$). The best-fit values of the associated delays (2000 being the reference year) are $\Delta t_1 = 138^{+27}_{-17}$ yr for Sgr C2 and $\Delta t_2 = 243^{+20}_{-25}$ yr for all other clouds (Sgr C1, C4, and B2). As the systematics discussed before may affect these values, we repeated the same analysis in the $Z = 1.3$ case. We found again that the two-flare scenario is preferred, and the delays are now $\Delta t_1 = 111^{+14}_{-11}$ yr and $\Delta t_2 = 204^{+24}_{-16}$ yr.

Another important assumption of the model is the cloud density profile. However, as stated in Sect. 4.1, alternative Gaussian profiles are statistically less good, and in any case, they cause the clouds to lie farther apart. This would be even more

inconsistent with a single-event scenario. Therefore our conclusions are rather robust against systematic effects and the values obtained in the $Z = 1.3$ case provide an estimate of the systematic uncertainty in the age determination of the outbursts.

The finding that Sgr C2 is illuminated by a second event is further supported by the two distinct variation patterns that can be identified in the light curves derived in Sect. 3. The time behaviours of Sgr C2 and Sgr C4 are indeed very different, one exhibiting a sudden rise and fall in about 2005, while the other decreases smoothly during the entire period. Even assuming that the Fe Kα emission in Sgr C2 peaked in about 2003, the illumination duration barely exceeds eight years. Because of the delay due to the propagation, the timescale of the associated flare has to be substantially shorter (i.e. a few years). Conversely, the light curve of Sgr C4 suggests a considerably longer timescale (ten years at least). This difference strongly supports the two-event scenario. Interestingly, Terrier et al. (2018) reported a trend for Sgr B2 very similar to the trend of Sgr C4, which is an important hint that these two clumps may be witnessing the same event. Although the light curve of Sgr C1 shows no evidence of a comparable linear decrease, the imaging analysis makes it clear that it is also illuminated by a long outburst (whose duration is estimated to ~20 yr by Terrier et al. 2018). As a consequence, the evidence in support of the two-event scenario does not come from position determination alone, but also from consistent patterns of variation found in the images and the light curves.

5. Discussion and conclusion

Sgr C is a much more complex region than Sgr B2. It notably hosts a SNR candidate that might be interacting with molecular material, as well as two nearby pulsar wind nebula candidates. As a consequence, this site is expected to be a good candidate for the cosmic-ray irradiation scenario. However, we were able to provide significant evidence of variability of the Fe Kα emission in all considered subregions. In this regard, it should be noted that Sgr C2 is located very close to the sharp edge of G359.41−0.12 (Chuard et al. 2017), which is a possible interaction region of the SNR candidate with molecular gas, that is, a candidate site for intense cosmic-ray production. Despite this, Sgr C2 is the clump for which we have the strongest evidence of short-term variability. This result, along with the consistent interpretation given in Sect. 4.1, is a very strong argument in favour of the reflection scenario. This does not exclude the possibility that LECR production may still contribute to the nearly constant level of background emission (see Fig. 2), however.

We propose that Sgr C1, C4, and B2 were illuminated by the same event that took place about 240 years before present[1] and lasted at least a decade. Additionally, we find that Sgr C2 was likely illuminated by a second flare that took place about 100 yrs later and lasted no longer than a few years. These results, which rely on imaging analysis, light-curve extraction, and three-dimensional position determination using a Monte Carlo spectral model, appear to be consistent with previous works that used different approaches. The most recent flare we report may be the same as the 110-year-old outburst described by Churazov et al. (2017), based on the comparison of time and space structure functions of the emission of a part of the Sgr A molecular complex. Furthermore, our findings are in very good agreement with the two-event scenario proposed by Clavel et al. (2013) for the Sgr A complex. As a result, the long flare seen in Sgr C1, C4, and B2 may be the same as the one seen by these authors in the molecular clouds known as MC1, MC2, and G0.11−0.11, while the short event seen in Sgr C2 may be the same as the one they see in the Bridge. Since we are able, for the first time, to assign an approximate date to these outbursts, we can infer the possible locations of the clumps in Sgr A. If the Bridge were indeed illuminated by the same flare as Sgr C2, the z-coordinates (as defined in Fig. 4) of its subregions Br1 and Br2 would thus be in the range of $z \sim 5$−25 pc. Similarly, assuming that MC1, MC2, and G0.11−0.11 recently witnessed the 240-year-old flare, their z-coordinates would thus be in the range of $z \sim 20$−45 pc. Following this approach, these predictions can be considered a test of the two-event scenario.

We are able to provide only lower limits on the luminosity of the associated outbursts. The implied luminosity varies with the inverse square of the radius of the cloud, assumed spherical, which is very poorly constrained. We used the size of the spectral extraction region instead, meaning that we clearly underestimate the luminosity. Moreover, clouds may not be fully illuminated, contrary to what we assume. It is also probable that we do not have data that match the time of maximum emission. Bearing this in mind, the X-ray luminosity (2–10 keV) of the two events illuminating Sgr C is estimated to be at least a few 10^{38} erg s^{-1}, and perhaps significantly higher (up to a few 10^{39} erg s^{-1}). As was extensively discussed in Clavel et al. (2013) for the Sgr A complex, Sgr A⋆ is the best candidate to account for the luminosity, spectral index, and flare duration required to explain the Fe Kα emission observed in Sgr C and to consistently illuminate both sides of the CMZ in three independent molecular complexes. The two flares we report could be due to stochastic variations of the accretion rate (Cuadra et al. 2008) or tidal disruption events (TDE; see e.g. Zubovas et al. 2012). While the constraints we place on their age and frequency may help in investigating their origin, both further regular monitoring of the Fe Kα emission of the CMZ and greater modelling efforts are still needed to ultimately unveil the past light curve of Sgr A⋆.

Acknowledgements. This research has made use of data obtained with *XMM-Newton*, an ESA science mission with instruments and contributions directly funded by ESA Member States and NASA, and from the *Chandra* Data Archive, as well as software provided by the *Chandra* X-ray Center (CXC) in the application packages CIAO, ChIPS, and Sherpa. The authors acknowledge the Centre National d'Études Spatiales (CNES) for financial support. G.P. acknowledges support from the Deutsches Zentrum für Luft- und Raumfahrt (DLR).

[1] The time delay due to the propagation of light from the Galactic centre to Earth (~26 000 yr) is not considered here.

References

Anantharamaiah, K. R., Pedlar, A., Ekers, R. D., & Goss, W. M. 1991, MNRAS, 249, 262
Baganoff, F. K., Maeda, Y., Morris, M., et al. 2003, ApJ, 591, 891
Balick, B., & Brown, R. L. 1974, ApJ, 194, 265
Boehle, A., Ghez, A. M., Schödel, R., et al. 2016, ApJ, 830, 17
Capelli, R., Warwick, R. S., Porquet, D., Gillessen, S., & Predehl, P. 2011, A&A, 530, A38
Capelli, R., Warwick, R. S., Porquet, D., Gillessen, S., & Predehl, P. 2012, A&A, 545, A35
Chatzopoulos, S., Fritz, T. K., Gerhard, O., et al. 2015, MNRAS, 447, 948
Chuard, D., Terrier, R., Goldwurm, A., et al. 2017, in The Multi-Messenger Astrophysics of the Galactic Centre, eds. R. M. Crocker, S. N. Longmore, & G. V. Bicknell, IAU Symp., 322, 208
Churazov, E., Khabibullin, I., Sunyaev, R., & Ponti, G. 2017, MNRAS, 465, 45
Clavel, M., Terrier, R., Goldwurm, A., et al. 2013, A&A, 558, A32
Clavel, M., Soldi, S., Terrier, R., et al. 2014, MNRAS, 443, L129
Cuadra, J., Nayakshin, S., & Martins, F. 2008, MNRAS, 383, 458
Cuadra, J., Nayakshin, S., & Wang, Q. D. 2015, MNRAS, 450, 277
Davies, B., Origlia, L., Kudritzki, R.-P., et al. 2009, ApJ, 694, 46

Degenaar, N., & Wijnands, R. 2013, in Feeding Compact Objects: Accretion on All Scales, eds. C. M. Zhang, T. Belloni, M. Méndez, & S. N. Zhang, IAU Symp., 290, 113
Dogiel, V., Cheng, K.-S., Chernyshov, D., et al. 2009, PASJ, 61, 901
Freeman, P., Doe, S., & Siemiginowska, A. 2001, in Astronomical Data Analysis, eds. J.-L. Starck, & F. D. Murtagh, Proc. SPIE, 4477, 76
Fruscione, A., McDowell, J. C., Allen, G. E., et al. 2006, in Proc. SPIE Conf. Ser., 6270, 62701
Garmire, G. P., Bautz, M. W., Ford, P. G., Nousek, J. A., & Ricker, Jr., G. R. 2003, in X-Ray and Gamma-Ray Telescopes and Instruments for Astronomy, eds. J. E. Truemper, & H. D. Tananbaum, Proc. SPIE, 4851, 28
Gehrels, N. 1986, ApJ, 303, 336
Genzel, R., Eisenhauer, F., & Gillessen, S. 2010, Rev. Mod. Phys., 82, 3121
Inui, T., Koyama, K., Matsumoto, H., & Tsuru, T. G. 2009, PASJ, 61, S241
Koyama, K., Maeda, Y., Sonobe, T., et al. 1996, PASJ, 48, 249
Koyama, K., Hyodo, Y., Inui, T., et al. 2007, PASJ, 59, 245
Koyama, K., Inui, T., Matsumoto, H., & Tsuru, T. G. 2008, PASJ, 60, S201
LaRosa, T. N., Kassim, N. E., Lazio, T. J. W., & Hyman, S. D. 2000, AJ, 119, 207
Legendre, L., & Legendre, P. 1998, Numerical Ecology, Developments in Environmental Modelling (Elsevier Science)
Liszt, H. S. 1985, ApJ, 293, L65
Liszt, H. S., & Spiker, R. W. 1995, ApJS, 98, 259
Molinari, S., Bally, J., Noriega-Crespo, A., et al. 2011, ApJ, 735, L33
Mori, K., Hailey, C. J., Krivonos, R., et al. 2015, ApJ, 814, 94
Morris, M., & Serabyn, E. 1996, ARA&A, 34, 645
Mościbrodzka, M. 2017, in The Multi-Messenger Astrophysics of the Galactic Centre, eds. R. M. Crocker, S. N. Longmore, & G. V. Bicknell, IAU Symp., 322, 43
Muno, M. P., Bauer, F. E., Bandyopadhyay, R. M., & Wang, Q. D. 2006, ApJS, 165, 173
Muno, M. P., Baganoff, F. K., Brandt, W. N., Park, S., & Morris, M. R. 2007, ApJ, 656, L69
Murakami, H., Koyama, K., Tsujimoto, M., Maeda, Y., & Sakano, M. 2001, ApJ, 550, 297
Nakajima, H., Tsuru, T. G., Nobukawa, M., et al. 2009, PASJ, 61, 233
Neilsen, J., Nowak, M. A., Gammie, C., et al. 2013, ApJ, 774, 42
Nobukawa, M., Tsuru, T. G., Takikawa, Y., et al. 2008, PASJ, 60, S191
Nobukawa, M., Ryu, S. G., Tsuru, T. G., & Koyama, K. 2011, ApJ, 739, L52
Ponti, G., Terrier, R., Goldwurm, A., Belanger, G., & Trap, G. 2010, ApJ, 714, 732
Ponti, G., Morris, M. R., Terrier, R., & Goldwurm, A. 2013, in Cosmic Rays in Star-Forming Environments, eds. D. F. Torres, & O. Reimer, Astrophysics and Space Science Proceedings, 34, 331
Ponti, G., De Marco, B., Morris, M. R., et al. 2015, MNRAS, 454, 1525
Ponti, G., George, E., Scaringi, S., et al. 2017, MNRAS, 468, 2447
Ryu, S. G., Nobukawa, M., Nakashima, S., et al. 2013, PASJ, 65, 33
Sawada, T., Hasegawa, T., Handa, T., & Cohen, R. J. 2004, MNRAS, 349, 1167
Smith, R. K., Brickhouse, N. S., Liedahl, D. A., & Raymond, J. C. 2001, ApJ, 556, L91
Snowden, S. L., Mushotzky, R. F., Kuntz, K. D., & Davis, D. S. 2008, A&A, 478, 615
Strüder, L., Briel, U., Dennerl, K., et al. 2001, A&A, 365, L18
Sunyaev, R., & Chuarzov, E. 1998, MNRAS, 297, 1279
Sunyaev, R. A., Markevitch, M., & Pavlinsky, M. 1993, ApJ, 407, 606
Tatischeff, V., Decourchelle, A., & Maurin, G. 2012, A&A, 546, A88
Terrier, R., Ponti, G., Bélanger, G., et al. 2010, ApJ, 719, 143
Terrier, R., Clavel, M., Soldi, S., et al. 2018, A&A, in press, DOI: 10.1051/0004-6361/201730837
Tsuboi, M., Handa, T., & Ukita, N. 1999, ApJS, 120, 1
Tsuru, T. G., Nobukawa, M., Nakajima, H., et al. 2009, PASJ, 61, 219
Turner, M. J. L., Abbey, A., Arnaud, M., et al. 2001, A&A, 365, L27
Walls, M., Chernyakova, M., Terrier, R., & Goldwurm, A. 2016, MNRAS, 463, 2893
Wang, Q. D., Nowak, M. A., Markoff, S. B., et al. 2013, Science, 341, 981
Worrall, D. M., Marshall, F. E., Boldt, E. A., & Swank, J. H. 1982, ApJ, 255, 111
Yan, Q.-Z., Walsh, A. J., Dawson, J. R., et al. 2017, MNRAS, 471, 2523
Yuan, Q., & Wang, Q. D. 2016, MNRAS, 456, 1438
Yusef-Zadeh, F., Law, C., & Wardle, M. 2002, ApJ, 568, L121
Yusef-Zadeh, F., Muno, M., Wardle, M., & Lis, D. C. 2007, ApJ, 656, 847
Zhang, S., Hailey, C. J., Mori, K., et al. 2015, ApJ, 815, 132
Zubovas, K., Nayakshin, S., & Markoff, S. 2012, MNRAS, 421, 1315